Electrical and mechanical stability of flexible, organic electrolyte-gated transistors based on iongel and hydrogels

ARTICLE

Electrical and mechanical stability of flexible, organic electrolyte-gated transistors based on iongel and hydrogels

Mona Azimi [a], Arunprabaharan Subramanian [a], Jiaxin Fan[a], Francesca Soavi [b] and Fabio Cicoira*[a]

Received 00th January 20xx,
Accepted 00th January 20xx
DOI: 10.1039/x0xx00000x

Electrolyte-gated transistors (EGTs) have been widely investigated for applications in bioelectronics owing to their low operating voltage and mixed ionic-electronic conduction. The ion-gating media play a primary role in determining the operating voltage and electrical stability of these devices. In this study, we employed an iongel based on an ionic liquid and hydrogels based on polyvinyl alcohol (PVA) as the gating media for EGTs using an organic semiconductor, poly(N-alkyldiketopyrrolo-pyrrole-dithienylthieno[3,2-b]thiophene) (DPP-DTT), as the channel material. The device characteristics revealed that iongel-gated transistors showed superior electrical stability over hydrogel-gated transistors because hydrogels undergo dehydration over time. After 65 cycles of pulse measurements, the drain current of the iongel-gated devices did not show any significant change, whereas it decreased to ~50 % of the initial value for the hydrogel-gated devices. By adding glycerol as an anti-dehydrating agent, the current decreased by only ~10 % under the same conditions, demonstrating improved operational stability. Finally, we fabricated flexible EGTs on polyethylene terephthalate (PET), which can be operated under different bending radii.

Introduction

Electrolyte-gated transistors (EGTs), which exploit mixed ionic-electronic transport, have applications in flexible and printed electronics, bioelectronics, and neuromorphic devices.[1, 2] EGTs can be operated at low voltages owing to the high electrical double-layer capacitance at the semiconductor/electrolyte interface. Different types of semiconductors have been used for EGTs, including organic small molecules and polymers, carbon nanomaterials, and metal oxides.[3, 4] A variety of materials are used for EGTs gating media, including aqueous saline solutions, ionic liquids, polymer electrolytes, polyelectrolytes, iongels and hydrogels.[5-7] These materials differ in their physical state (e.g., solid, gel, or liquid), electrochemical stability, ionic conductivity, and mechanical properties. Aqueous electrolytes, which are used in most bioelectronic applications, have the disadvantages of limited electrochemical stability (~1.2 V) and rapid evaporation, leading to device degradation. Ionic liquids have a negligible evaporation rate and a wide electrochemical stability window (~3 V).[8] However, their liquid state remains an obstacle for integration into solid-state devices. Solid-state gating can be achieved with polymer electrolytes, that is, salts dispersed in a polymer matrix; polyelectrolytes, that is, macromolecules bearing ionic groups; iongels, that is, mixtures of ionic liquids with polymers; and hydrogels, that is, cross-linked three-dimensional networks of hydrophilic polymeric chains that swell in water.[8] Among these materials, iongels and hydrogels are the most suited for flexible and stretchable EGTs because of their softer nature and superior mechanical properties.[9, 10] Iongels show negligible evaporation rate, wide electrochemical stability window, and, owing to their hydrophobic nature, are compatible with most organic semiconductors. Moreover, they exhibit versatility for processing via printing techniques, [11, 12] and can be utilized as ion-exchange layers to facilitate the penetration of ions into the hydrophobic semiconductor material.[13] Hydrogel electrolytes are of particular interest for flexible electronics, since their crosslinked polymer structure enables high water absorption and mechanical softness.[14] Hydrogels based on biomaterials such as gelatin, cellulose and agarose or biodegradable materials, such as polyvinyl alcohol (PVA), have been used for the fabrication of sustainable devices.[15, 16] PVA hydrogels have been used as healable electrolytes, which retrieved 95% of their initial ion sensitivity after healing and showed 86% retention of drain current after 1000 cycles.[17] The major concern about hydrogels is their dehydration over time, which impacts the device electrical stability. The dehydration process can be inhibited by incorporating non-volatile organic polyols (e.g., ethylene glycol, glycerol) to improve the water retention ability via formation of multiple hydrogen bonds, thus permitting the fabrication of EGTs suitable for long-term electrophysiological monitoring.[18] There are two methods to introduce organic solvents in the formulation of hydrogels: i) gelation of the matrix polymer in a mixture of water and organic solvents, and ii) solvent displacement, achieved by immersion of the hydrogel in polyol-based solvents.[19]

To expand the use of EGTs for practical applications, it is critical to improve their electrical stability over time, which mostly depends on active materials, ion-gating media, and metal contacts. Most studies

[a] Department of Chemical Engineering, Polytechnique Montréal, Montréal, Québec, H3T 1J4, Canada, Email: fabio.cicoira@polymtl.ca
[b] Dipartimento di Chimica "Giacomo Ciamician", Università di Bologna, Via Selmi 2, Bologna 40126, Italy.

Electronic Supplementary Information (ESI) available: [details of any supplementary information available should be included here]. See DOI: 10.1039/x0xx00000x

to date have focused on the chemical stability of active materials or metal electrodes for long-term applications,[20, 21] while the influence of different gating media on the electrical stability of EGTs has yet to be sufficiently explored. Non-aqueous (semi-solid) electrolytes present unique advantages over their aqueous counterparts for applications in flexible and stretchable electronics. Possible applications include wearable devices for health monitoring, artificial skin and implantable electronics. These applications require continuous stability over time, as well as intimate contact with curved surfaces that undergo frequent mechanical deformation. Aqueous electrolytes typically do not meet these requirements owing to their fluid nature and high volatility under ambient conditions.

Dasgupta *et al.*,[22] reported the long-term stability of EGTs based In_2O_3 using different types of polymer electrolytes. The polymer electrolytes were composed of PVA (molecular weights of 13k and 89k), dimethyl sulfoxide (DMSO), propylene carbonate (PC), and lithium perchlorate ($LiClO_4$). They showed that high-molecular-weight PVA improved the stability of hydrogels owing to better water uptake. It has been reported that the normalized transconductance of EGTs gated with high molecular weight PVA changed from 51 ± 19 (for as prepared device) to 51 ± 17 and 54 ± 14 µS µm^{-1} after one month and 8 months, respectively. The normalized transconductance for low molecular weight PVA decreased from 57 ± 16 (for as prepared device) to 50 ± 13 and 47 ± 17 µS µm^{-1} after one month and 8 months post-fabrication, respectively. However, the operational stability of EGTs based on organic semiconductors and the use of different gating media has not yet been reported.

Zaumseil *et al.*[23] found that the replacement of the acidic hydrogen of the imidazolium salt with a methyl group improved the stability of ZnO based EGTs. The operational stability of EGTs based on DPP-DTT in aqueous electrolytes has been reported previously. After 5 days in ambient conditions, the initial mobility value of 0.15 cm^2 V^{-1} s^{-1} decreased by less than 10 %, while similar devices based on poly(3-hexylthiophene) (P3HT) showed a 30 % decrease.[24] Electrical stability of iongel gated EGTs based on pristine P3HT and its mixture with ionic liquid (1-Ethyl-3-methylimidazolium bis(trifluoromethylsulfonyl)imide ([EMIM][TFSI])) has also been studied. The hole mobility decreased by 70 % for neat P3HT devices after 150 switching cycles, whereas the mobility of EGTs based on the blend of semiconductor with ionic liquid retained 90 % of its initial value.[25]

In this study, we used hydrogel ion-gating media for the DPP-DTT-based EGTs. We investigated the electrical stability of EGTs by focusing on the effects of ion-gating media, including iongels and hydrogels. The iongel was based on poly(vinylidene fluoride-co-hexafluoropropylene) (PVDF-HFP) (IUPAC name:1,1-difluoroethene, 1,1,2,3,3,3-hexafluoroprop-1-ene) and the ionic liquid ([EMIM][TFSI]). PVDF-HFP was selected as the matrix polymer owing to its film-forming ability and high tensile strength. Hydrogels are based on PVA, a sustainable material whose gelation occurs through a freezing/thawing process, leading to the formation of hydrogen bonds without additional chemical crosslinkers. We observed superior electrical stability for iongel-gated devices compared to devices gated by hydrogels, which, without an anti-dehydrating agent, exhibited electrical degradation over time owing to the fast evaporation of water. The addition of high-boiling point glycerol to the hydrogel formulation significantly improved the electrical stability of the devices. Furthermore, changes in the drain current and mobility under different bending radii were monitored to evaluate the flexibility of the devices. This study contributes to the understanding of the effect of different gating media on the electrical characteristics and operational stability of EGTs based on organic semiconductors. The development of flexible EGTs with reasonable operational stability promises the future application of novel flexible electronics.

Results and discussion

Structural and Topographical Characterization

The chemical structures of the materials used for the EGTs and the device structure are shown in **Figure 1** (a side view of the device structure is shown in Figure S1a). The iongel (PVDF-HFP/IL) was a mixture of PVDF-HFP and [EMIM][TFSI] (Figure 1a). The hydrogels were mixtures of PVA and aqueous NaCl (0.5 M or 0.7M), with or without glycerol (Figure 1b). The hydrogel formulations are listed in **Table 1**. To evaluate the effect of ion-gating media on EGTs performance, we maintained the same device dimensions. To investigate the effect of glycerol on the electrical stability and performance of the devices, the composition of the swelling solution was varied.

Table 1. Chemical composition of hydrogels

Hydrogel	Swelling solution
PVA/W (0.5)	NaCl 0.5M in H_2O
PVA/W+Gl (0.5)	NaCl 0.5M in H_2O /glycerol (50/50) (%v/v)
PVA/W+Gl (0.7)	NaCl 0.7M in H_2O /glycerol (50/50) (%v/v)

The semiconductor DPP-DTT was used as the channel material (Figure 1c). The choice of semiconductor is critical for achieving electrical stability in the transistors. DPP-DTT exhibited stable transistor characteristics in aqueous electrolytes.[3, 24] Height micrographs obtained from atomic force microscopy (AFM) revealed that DPP-DTT films on Si/SiO_2 (Figure 1d) consist of well-ordered and homogeneously distributed lamellae, with a root mean square (rms) surface roughness of 3.5 ± 0.4 nm, which is similar to previously reported observations.[24, 26] The X-ray diffraction (XRD) pattern (Figure S1b) revealed semi-crystalline characteristics, with a first-order lamellar stacking peak (100) at 2θ= 4.65°, corresponding to an interlayer alkyl side chain distance of ~10 nm. This is in sufficient agreement with the findings of Lei *et al.*[27] and Zhang *et al.*,[28] who observed the (100) peak positioned at 2θ= 4.45°.

ARTICLE

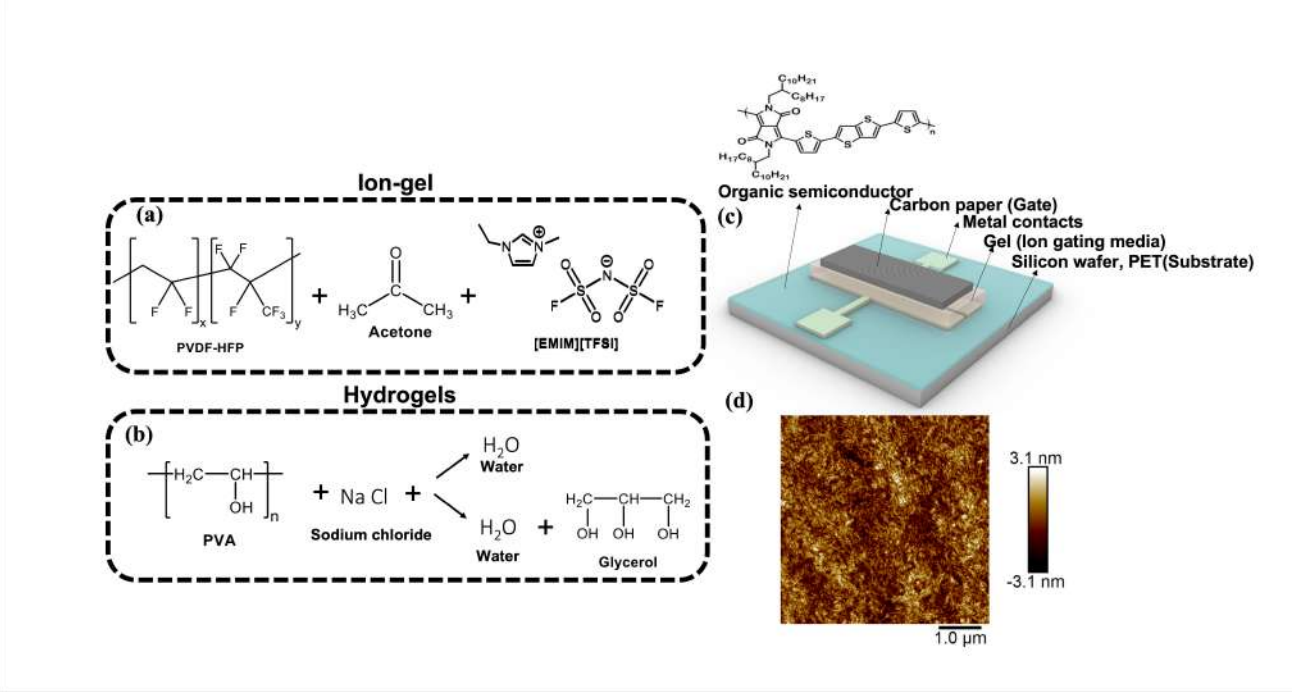

Figure 1. Molecular structures of the materials used for iongels (a) and hydrogels (b), scheme of device and molecular structure of the organic semiconductor (DPP-DTT) (c), AFM image of spin-coated DPP-DTT film on Si/SiO_2 substrate (d).

Electrochemical Properties of Iongel and Hydrogels

Electrochemical characterization of the ion-gating media was performed in a metal-insulator-metal (MIM) configuration (**Figure 2**a, see experimental section for details) to determine their ionic conductivity and capacitance, as well as stability over time. In MIM structures, the electrolyte is sandwiched between two conductor layers. Although Au is commonly used as the contact material in such structures, other conductive materials such as indium tin oxide (ITO) can be used. For example, Kim *et al.*[25] used ITO as the bottom contact and aluminum as the top contact. We chose Au as the bottom electrode and conductive carbon paper coated with activated carbon as the top electrode. This materials, which has a high surface area, high capacitance, and wide electrochemical stability window, is commonly used as a gate electrode in EGTs,[4, 7, 29, 30] and can be directly laminated on the gel electrolyte without the need of thermal evaporation. The Nyquist plots (imaginary component, Z_i, versus the real component of impedance, Z_r) show tilted straight lines that are related to the typical behavior of electrolytes in contact with the solid electrodes. The high-frequency region of the Nyquist plots (Figure 2b) does not show a semicircle, which indicates non-Faradaic processes at the gel/electrode interface.[31, 32] The behavior of Z_r at high frequencies (Figure 2c) reveals that the equivalent series resistance (ESR) of the iongel and PVA/W(0.5) are almost similar and lower than those of glycerol-containing hydrogels. The ESR value includes the contributions of the bulk resistance of the electrolyte and the interfacial resistance between the electrolyte and the electrode. The absence of a semi-circular region at high frequencies (10^5 Hz) indicates that the interfacial resistance is negligible compared with the bulk resistance.[33, 34] The higher ESR value in glycerol-based hydrogels is likely due to the presence of glycerol, which is an insulating material. Figure 2d shows the impedance versus the frequency of the electrolytes. The decrease in impedance by increasing the frequency is related to the formation of an electric double-layer.[33, 35] The impedance at high frequencies, which is related to the bulk resistance of electrolytes, is higher for hydrogels containing glycerol. For all gels, the phase angle is ~-45° or lower at frequencies lower than 10 Hz (Figure 2e), which indicates a non-ideal capacitive behavior (a phase angle of -90° indicates purely capacitive behavior). The iongel shows higher phase angles at low frequency (1 Hz) with respect to hydrogels. For hydrogels with and without glycerol and a lower concentration of NaCl (0.5 M) the phase angle was ~-50°. At higher NaCl concentration (0.7 M), the phase angle increased to ~-60°, which indicates an improved capacitive behavior. At frequencies higher than 10 Hz, the hydrogels with glycerol showed lower phase angles, likely due to the hindrance effect of glycerol, which inhibits double layer formation.[35]

ARTICLE

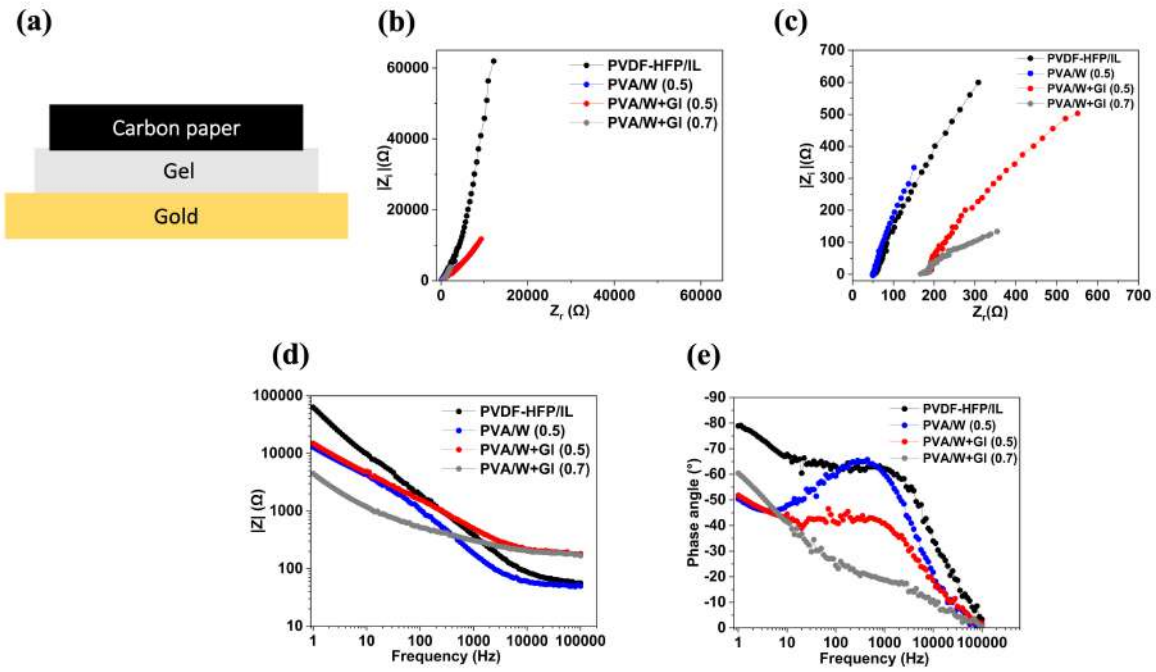

Figure 2. MIM structure (a), Nyquist plots of gels (b), magnified Nyquist plots at high frequencies (c), Bode plot (impedance versus frequency) (d), Bode plot (phase angle versus frequency) The sample compositions are listed in Table 1.

We extracted the ionic conductivity and capacitance of the MIM assembled with gels from Equations (1) and (2) (experimental section). The values, summarized in **Table 2,** are comparable with those reported for state-of-the-art systems featuring iongels and hydrogels (Table S1).[10, 12, 25, 36-38] Our measurements yielded the capacitance of the electric double layer at the interface between the Au electrode (working electrode) and the electrolyte, which does not depend on the thickness of the electrolyte.[39, 40] Capacitance values from the MIM structure provide insight into the capacitive behavior of electrolytes in EGTs. However, they are not directly related to the device performance (see next paragraph for details). The ionic conductivity depends on the ion concentration and mobility, as well as on the viscosity of the material.[41] Hydrogels show higher ionic conductivity than iongels because the large amount of water present in the material (typically over 70 %) facilitates ion transport.[42, 43] The addition of glycerol increases the viscosity, leading to a decrease in ionic conductivity.[44, 45] The equivalent circuit model of our system (inset of Figure S2) consists of a resistor and a constant phase element (CPE) in series. Resistance includes both ionic and electronic contributions. The CPE accounts for the electric double-layer, and α is a parameter accounting for the electrolyte behavior (α=1 corresponds to an ideal capacitor). The parameters obtained from the fitting are listed in Table S2. The iongel and PVA/W(0.5) showed a resistance value lower than that of glycerol-containing hydrogels. The higher resistance observed in hydrogels containing glycerol is related to the presence of glycerol, which is an insulating material. Comparing the α values of the electrolytes reveals that the iongel (α~0.8) behaves more like an ideal capacitor than the hydrogels (α~0.5). This is likely due to the presence of water molecules in hydrogels, which inhibits ideal capacitor behavior. The highest CPE value is found for PVA/W+Gl(0.7), in agreement with its highest capacitance.

Table 2. Ionic conductivity and capacitance values of MIM devices obtained from EIS measurements. (The thicknesses of iongel and hydrogels are ~130 µm and 1000 µm, respectively.) The values were averaged for three samples, and the errors represent the standard deviation.

Gels	Ionic conductivity (mS cm^{-1})at 10^5Hz	Effective Capacitance (µF cm^{-2}) at *f*=1Hz
PVDF-HFP/IL	0.6±0.1	4.5±0.8
PVA/W (0.5)	9.4±.3.5	28.6±7.9
PVA/W+Gl (0.5)	2.7±0.3	30.5±6.5
PVA/W+Gl (0.7)	3.1±0.5	51.2±15.4

ARTICLE

Characterization of Iongel and Hydrogel Gated Transistors

The electrical characteristics of the iongel and hydrogel-gated transistors are shown in **Figure 3.** The figures of merit are summarized in **Table 3** (values averaged for six devices and error bars corresponding to standard deviation). The output curves show p-type enhancement mode operation (Figure 3a, a b, c, and d)). The transfer curves ($|I_d|$ versus V_d) in the saturation region (V_d= -0.8 V) show ON-OFF ratios of ~10^2-10^3 between 0 and -1 V, in agreement with reports for other EGTs based on DPP-DTT (see Table 3 for details).[24] The transconductance ($g_m = \partial I_d/\partial V_a$) depends on the device geometry, applied voltage, charge carrier mobility, and capacitance.[46] The transconductance versus V_g plots (Figure 3e, f, g, and h) reveal that the highest value is shown by the PVA/W+Gl (0.7) gated device. This result can be ascribed to the high capacitance of this gating medium, which leads to large current modulation and a higher ON state current. The transfer curves in the linear region (V_d= -0.2 V) are shown in Fig. S3. Smoother transconductance curves were obtained at lower scan rates (10 mV s^{-1}, Figure S4). The gate current versus gate voltage plots are shown in Figure S5. The leakage current was approximately three orders of magnitude smaller than the drain current. Patterning the semiconductor, gel electrolyte, or concentric source-drain electrodes is a possible strategy to decrease the gate leakage current. [47-49] The leakage current in our devices can be attributed to the unpatterned semiconductor layer, which has been spin coated all over the surface (1 cm×1 cm). In terms of the configuration of devices, it has been shown that the top gate configuration has higher gate leakage current with respect to the planar gate configuration. [50]

The charge carrier density and mobility values were calculated using Eqs. (3) and (4). The values of transconductance and mobility are among the highest reported for state-of-the-art organic EGTs.[3, 24, 25, 37, 51] Specifically for EGTs based on DPP-DTT semiconductor, Zhang *et al.* [24] obtained mobility and ON-OFF ratio of 0.15 $cm^2\ V^{-1}\ s^{-1}$ and 3×10^2, respectively, using s NaCl solution as an electrolyte. Tong *et al.* [3] reported a mobility of 0.18 $cm^2\ V^{-1}\ s^{-1}$ and an ON-OFF ratio of 3×10^3 for EGTs based on DPP-DTT using deionized water as an electrolyte. PVA/W (0.5) gated transistors exhibited a lower drain current with respect to devices gated with glycerol-based hydrogel, which can be explained by the rapid dehydration of the hydrogel (note that the time interval between the assembly of the device and measurement was the same (20 min) for all devices). Devices based on PVA/W+Gl (0.7) hydrogels showed the best performance in terms of output current and transconductance owing to the high capacitance of the ion gating medium.

The capacitance values reported for MIM structures are related to the electrolyte/gold-electrode interface. However, in the transistor configuration, two electrical double layer capacitors are formed: one at the gate/electrolyte interface and the other at the semiconductor/electrolyte interface. As these two capacitors are in series, the total capacitance in the transistor configuration is given by : $C_{total} = \frac{1}{1/C_{ch} + 1/C_g}$, where C_{ch} is the capacitance at the interface between the channel and the electrolyte and C_g is the capacitance at the interface between the electrolyte and the gate electrode.[52] In the transistor configuration, the drain current is directly proportional to C_{tot}. Thus, we cannot expect to observe a proportional relationship between the capacitance obtained from the MIM structure and drain current of the transistor.

We obtained the hysteresis width, that is, the gate voltage shift corresponding to the reference drain current in the forward and backward scans, according to Equation (5). Normally, the average value between the maximum and minimum drain currents in the transfer curves (-2 mA for PVA/W (0.5) and -5mA for PVA/W+Gl(0.7)) is considered as the reference drain current to evaluate the hysteresis. The PVA/W (0.5)-gated devices had a larger hysteresis width (~0.3 V) than those gated with glycerol-containing gels (~0.1 V). The hysteretic behavior in EGTs is due to the slow movement of ions in the electrolyte to form an electric double layer at the gate/electrolyte and electrolyte/semiconductor interfaces. In iongel or hydrogel electrolytes ions have lower conductivity (10^{-5}- 10^{-2} S/cm) compared to aqueous electrolytes (e.g., 0.01 M NaCl aqueous solution with 10^{-3} S/cm).[40] The size of ions is another parameter affecting the hysteresis of EGTs. Larger ions have poor polarization efficiency and slower movement, which contribute to higher hysteresis.[53] In practical applications, electrolytes with higher ionic conductivity (aqueous electrolytes) and small ion size could have a significant effect on the reduction of hysteresis. In addition to the electrolyte properties, the characteristics of the semiconducting film, such as the morphology and thickness of the film, influence the hysteresis of EGTs.[54] The position and area of the gate electrode also determine the hysteresis; a larger gate electrode and closer position to the channel result in smaller hysteresis.[55] So, hysteresis is less pronounced in the top-gated configuration than in the side-gated configuration. We observed hysteresis for both the iron-gated and hydrogel-gated devices. However, the hysteresis for hydrogels without an anti-dehydrating agent was higher than that for glycerol-based hydrogels because of the high rate of water dehydration. The dried hydrogel can show poor polarization efficiency and slow migration of ions within the electrolyte to reach the electrolyte/semiconductor.[56] So, the higher hysteresis of the PVA/W (0.5) transistor is due to the instability and degradation in the performance of the device due to the dehydration of the hydrogel.

EGTs have two operating regimes for EGTs; electrostatic and electrochemical. In the electrostatic mode, the channel material is not permeable to ions, and by applying a gate voltage, ions accumulate at the interface of the semiconductor/electrolyte, and an electric double-layer forms at the interface. In the electrochemical mode, ions can permeate the bulk of the semiconductor, so doping

can occur in three dimensions. Electrochemical doping leads to reversible electrochemical oxidation and reduction reactions.[40]

To further investigate and understand the working mechanism of EGTs with ion-gel electrolytes, we performed cyclic voltammetry (CV). CV is widely used to investigate the redox properties of materials (i.e., the redox potential and stability of redox states). Studying the interaction between the active material and the dopant agent reveals information about the doping mechanism. To investigate the electrochemical properties of semiconductors with semi-solid electrolytes, the metal/insulator (iongel)/semiconductor (MIS) structure is an appropriate configuration instead of a conventional electrochemical cell. In the MIS structure, the organic semiconductor is in contact with a semisolid electrolyte. Performing CV with this configuration revealed the redox properties of the semiconductor with the proposed electrolyte. In our experimental design, we first performed CV measurements using the MIM structure to study the electrochemical activity of the electrolyte in the applied potential range to eliminate interference. As expected, an almost capacitive behavior was observed for the MIM structure (Figure S6 a), indicating that there was no electron transfer between the iongel electrolyte and the Au electrode; hence, the process was non-faradaic. However, in the case of the MIS structure (Figure S6 (b)), we observed an almost reversible faradaic peak at V=0.5 V. In the forward scan, the anodic current peak was 25 µA, whereas in the backward scan, the cathodic current peak reached only -5 µA. The anodic and cathodic currents are not equal, which is attributed to the fact that only a fraction of the molecules that were oxidized in the forward scan were then reduced during the reverse scan. Principally, faradaic processes are paralleled by the insertion of ions to the bulk of the active material; however, considering the large size of [EMIM][TFSI] ions and well-ordered morphology of DPP-DTT, we hypothesize that the redox process is confined at the interface of the electrolyte and semiconductor film. Based on the electrochemical and transistor characterizations, the coexistence of interface-confined electrochemical doping and electrostatic doping is proposed.

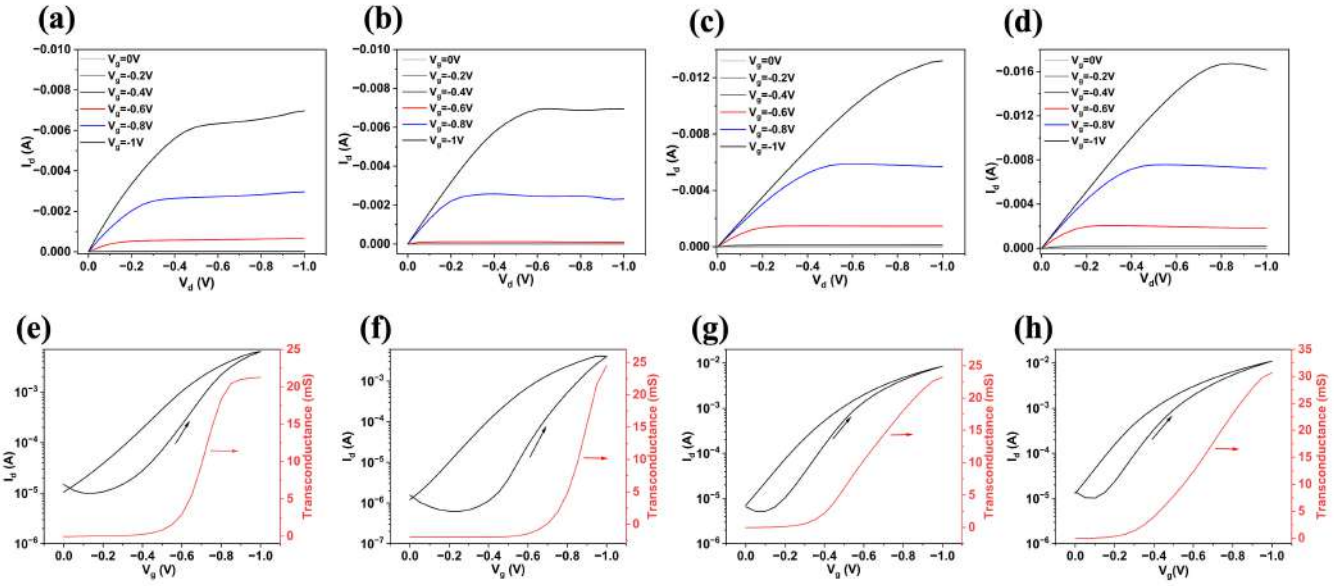

Figure 3. Output curves of PVDF-HFP/IL, PVA/W (0.5), PVA/W+Gl (0.5), and PVA/W+Gl (0.7) gated transistors (a, b, c, d) obtained at six different gate voltages (0 V<V_g< -1 V with interval of 0.2 V). Transfer curves (log scale) in the saturation region (V_d= -0.8 V) (right Y-axis represents transconductance (e, f, g, h). Scan rate is 50 mV s^{-1}.

Table 3. Figures of merit for iongel and hydrogel-gated transistors. The charge carrier density and mobility values were obtained using Eqs. (3) and (4), respectively. The values were averaged for the six devices, and the errors represent standard deviations.

Gel	Charge carrier density (cm^{-2})	Mobility (cm^2 V^{-1} s^{-1})	ON-OFF ratio	Threshold voltage (v)	g_m (mS)	I_d (mA) at V_g = -1V, V_d= -0.2V	I_d (mA) at V_g = -1V, V_d= -0.8 V
PVDF-HFP/IL	2.2±0.1 E14	0.79 ±0.07	~5×10^2	-0.6±0.1	25±4	2.2±0.6	6.6±1.2
PVA/W (0.5)	4.8±0.6 E14	0.60±0.19	~4×10^3	-0.6±0.1	22±3	3.1±0.8	5.2±1.4
PVA/W+Gl (0.5)	5.1±0.3 E14	0.88±0.10	~8×10^3	-0.5±0.2	30±5	3.8±0.5	11.4±0.7
PVA/W+Gl (0.7)	5.6±0.5 E14	1.12±0.17	~7×10^3	-0.5±0.2	34±5	4.5±0.6	14.9±1.1

Electrochemical stability of ion-gating media

To study the effect of different gating media on the electrical stability of EGTs, we evaluated the electrochemical stability of the ion-gating media over time using EIS. As shown in Figure S7a, the Nyquist plots of the iongel over two weeks did not change, and the real component of impedance at high frequency (Figure S7d), which correlates with ionic conductivity, did not change significantly. For PVA/W (0.5), the value of Z_r at high frequency (and therefore the ionic conductivity) doubled after 30 min and increased by a factor of four after 60 min (Figure S7 b, e), likely due to water evaporation. For the glycerol-containing hydrogels (Figure S7 c, f), the Nyquist plots remained stable over two days, which shows that the incorporation of glycerol was efficient in increasing the water retention ability of the hydrogel. In 3rd day the Z_r value at a high frequency increased by two times. Accordingly, the ionic conductivity decreased by 2 times.

Electrical stability of EGTs based on iongel and hydrogels

We evaluated the electrical stability of the iongel- and hydrogel-gated devices by measuring 20 consecutive transfer curves, sweeping V_g from 0 V to -1 V, and backward (**Figure 4**a-c). The iongel (PVDF-HFP/IL)-gated devices showed no significant changes in current, threshold voltage, and ON-OFF ratio over 20 cycles (Figure 4a).

Devices based on PVA/W (0.5) hydrogels show a ~45 % decrease in drain current and a threshold voltage shift from -0.7 V to -0.8 V after 20 cycles (Figure 4b). For PVA/W+Gl (0.7) hydrogel, the current decreased only by ~5 %, with no significant change in threshold voltage (Figure 4c). We further investigated the electrical stability (transient behavior) of the devices using square-wave pulse measurements varying V_g from 0 V to −0.8 V, with a pulse length of 5 s, at V_d = −0.2 V (Figure 4d-f). After 65 ON-OFF cycles (~1000 s), the PVDF-HFP/IL gel gated devices maintained ~98 % of their drain current (Figure 4d), whereas the PVA/W (0.5) gated devices exhibited a decline of ~50 % (Figure 4e). The devices gated with glycerol-containing hydrogels (Figure 4f, S8) maintained ~90 % of their initial current during 65 cycles. As DPP-DTT is stable in aqueous media, [24] the observed performance decrease is caused by the dehydration of the hydrogel. The fast dehydration of hydrogels without an anti-dehydrating agent is a weak point of these ion-gating media, which can be prevented, at least partially, by the addition of glycerol (normal boiling point of 290 °C). The effectiveness of glycerol in partially preventing dehydration was confirmed by measuring the normalized mass (m/m_0) (where m is the mass of the dehydrated hydrogel, and m_0 is its initial mass) versus time (Figure S9b). One hour after removal from the swelling solution, the hydrogel without glycerol lost ~45 % of its mass, whereas that containing glycerol only lost ~15 %. Optical images of freshly prepared hydrogels and 24 h after removal from the swelling solution (Figure S9a, top and bottom) show that the PVA/W (0.5) hydrogel completely dehydrated after one day, while PVA/W+Gl (0.7) retained its structure. Magnified five cycles of pulse measurements in the time scale of 200-250 s are shown in Figure S10 to highlight the switching properties of the devices, which are mainly governed by ionic transport and time of electric double-layer formation.[40] Iongel-gated transistor showed a slower switching speed with respect to the hydrogels, as highlighted by the transient curves (Figure S10a). For iongel-gated devices, the drain current did not reach the steady state in either the ON or OFF states after 5 s of gate bias application. This indicates slow kinetics for the processes of electric double-layer formation as a consequence of the slow ion motion of bulky $[TFSI]^-$ ions. For hydrogel-gated transistors, the OFF current stabilizes after a 5 s pulse at V_g= 0 V, while a longer time (> 5 s) is needed to stabilize the ON current (Figure S10 b,c). The faster switching OFF time of hydrogel-gated devices is due to the smaller size of the $[Cl]^-$ ions and facile ion transport toward the gate electrode in the OFF state. The electrical stability of EGTs was evaluated over a longer time span. The iongel-gated devices were stable for over two weeks without any significant change in the drain current (Figure S11a). Devices gated by PVA/W (0.5) showed a ~60 % decrease in the drain current within 1 h (Figure S11b). The addition of glycerol led to improved electrical stability, i.e., the drain current remained almost unchanged for 2 days and decreased by 40 % on 3rd day (Figure S11c).

ARTICLE

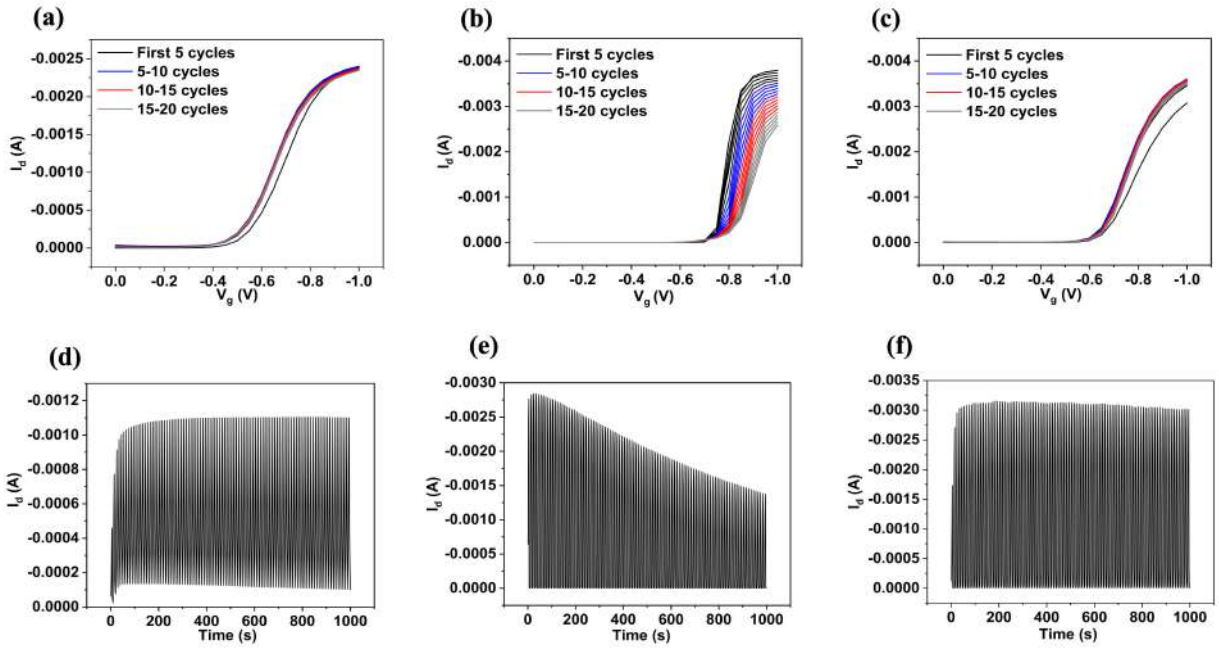

Figure 4. Sequence of 20 transfer curves (V_d =−0.2 V) for PVDF-HFP/IL, PVA/W (0.5) and PVA/W+Gl (0.7) gated transistor (a, b, c) (only forward scans are plotted for clarity); pulse measurements with V_d =−0.2 V and square pulse V_g varied from 0 to -0.8 V (pulse duration = 5 s) for PVDF-HFP/IL, PVA/W (0.5) and PVA/W+Gl (0.7) gated transistor (d,e, f).

Electrical characterization of EGTs in bent state

Gel electrolytes are of great interest for use in flexible electronic devices because of their superior mechanical properties compared to aqueous electrolytes. Semi-solid electrolytes, including iongels, hydrogels, and polymer electrolytes, have been reported for applications in organic and inorganic flexible and stretchable EGTs.[36, 57-59] Recently, Kim *et al.* reported fully stretchable OECTs based on PEDOT-PSS, using printed hydrogels as the gating media.[57] Biodegradable and biocompatible iongels have been utilized for flexible EGTs with an application for electrocardiogram recording.[36] Agarose based hydrogel have also been used to fabricate flexible pressure sensors with long-term stability and sensitivity in the low-pressure regime (for several hundred pascals).[9] Therefore, electrical measurements were performed under bending to evaluate the mechanical stability of gel-gated EGTs. Flexible EGTs were fabricated on polyethylene terephthalate (PET). The flexibility of the devices was evaluated by measuring the transfer curves in the linear region (V_d= -0.2 V) in the bent states (**Figure 5**). Bending radius of 20 mm and 10 mm corresponds to tensile strain of ~0.9 % and ~0.45 %, respectively (where tensile strain is defined as ε = D/2R, where D is the thickness of substrate (175 µm) and R is bending radius).[54] As DPP based polymer is potentially applicable for stretchable devices,[60] we assume that current changes during bending only depend on the gating media. PVDF-HFP/IL gated transistor showed a small change (less than 10 %) in the drain current upon bending (Figure 5a). For PVA/W (0.5) gated devices, the transfer curves reveal a significant decrease (~50 %) in drain current in the bent state (R~10 mm) with respect to the flat state (Figures 5b). The PVA/W+Gl (0.7) (Figure 5c) EGTs showed a slight decrease in the drain current in bent states with respect to the PVA/W (0.5) gated devices. As the iongel and PVA/W+Gl (0.7) gated transistors showed stable performance over time, the decrease in their drain current upon bending was mainly caused by mechanical effects. Since the time to perform the electrical characterization of devices in bent state is rather long (~40 minutes), in the case of PVA/W (0.5)-gated devices, the significant decrease in current in bent states is likely due to both mechanical effects and dehydration. The threshold voltage of iongel-gated devices did not change significantly upon bending, while that of hydrogel-gated devices increased by ~30%. The increased stability of iongel-gated devices upon bending can be explained by the stronger adhesion of the gating medium on the devices, as a result of its lower thickness and hydrophobicity. Figure 5d illustrates the changes in the hole mobility of the transistors when changing from a flat to bent state. There was no significant change in the mobility of the PVDF-HFP/IL-gated transistors. PVA/W (0.5) and PVA/W+Gl (0.7) gated

devices experienced ~50 % and ~10 % decreases in mobility values in bent state. These results suggest that DPP-DTT has reasonable flexibility, as reported elsewhere[61], and is a good candidate for other flexible electronic applications.

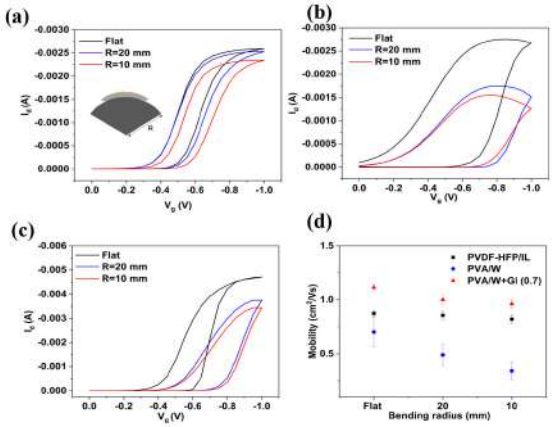

Figure 5. Transfer curves (V_d= -0.2 V) of PVDF-HFP/IL (inset is related to the scheme of bending) (a), PVA/W (0.5) (b), and PVA/W+Gl (0.7) (c) gated transistors in different bent states. Hole mobility of three different gel-gated transistors in bent and unbent conditions (error bars represent the standard deviation for three different samples).

Conclusions

In summary, we demonstrated EGTs based on a p-type ambient-stable DPP-DTT organic semiconductor using iongels and hydrogels as gating media. Devices based on iongels showed higher electrical stability than hydrogel-based devices and maintained 98 % of the initial current after 20 consecutive cycles. However, devices gated by hydrogels without an anti-dehydrating agent exhibited a 45 % decrease in drain current after 20 cycles owing to the dehydration of the hydrogel. The incorporation of glycerol into the hydrogel significantly improved its electrical stability and decreased the current by only 5 % after 20 cycles. We tested the electrical stability of the devices over a long period of time, and the ion-gel-gated transistor showed stable operation within 2 weeks. The hydrogels without an anti-dehydrating agent showed the weakest performance, where the drain current decreased by 60 % after 1 h compared to the initial measurement. Glycerol-based hydrogels showed improved electrical stability, and the drain current was stable for 2 days. Flexible EGTs fabricated on PET substrates are also investigated. No significant changes were observed in the electrical characteristics of the ion-gel-based devices in the bent state, which was attributed to the physicochemical stability of the iongel and its good adhesion to the substrate. We observed a significant drain current decline in the case of PVA/W(0.5) when compared to PVA/W+Gl (0.7), because the evaporation of water had a synergistic effect on the current drop in parallel with bending. Our results provide insights into the electrical stability of iongel and hydrogel-gated devices. Moreover, these findings pave the way for realizing the compositional formulation of non-volatile and environmentally friendly electrolytes for use as gating media in electrolyte-gated devices.

Experimental

Materials and methods

The organic semiconductor (DPP-DTT) was purchased from Ossila; chloroform ($CHCl_3$) was purchased from Acros Organics; PVDF-HFP (Mw~400,000, Mn~130,000) and PVA (Mw~89,000-98,000, 99+ % hydrolysed) were purchased from Millipore Sigma. The ionic liquid ([EMIM][TFSI]) (viscosity of 39.4 mPa·s and ionic conductivity of 6.63 $mS{\cdot}cm^{-1}$) was supplied by IoLiTec and purified under vacuum (~10^{-5} Torr) at 60 °C for 24 h before use. Carbon paper (Spectracarb 2050) coated with carbon ink was used as the gate electrode. The electrical resistivity of the carbon paper is 5.4 mΩcm (as declared by the supplier) and its roughness ~18 µm, as reported in the literature. [62] The Carbon ink contains activated carbon (Norit CA1, Millipore Sigma, 28 mg mL^{-1}), polyvinylidene fluoride (PVDF, Millipore Sigma) (IUPAC name: 1,1-difluoroethene), Nafion, and N-methyl pyrrolidone (NMP, Fluka, >99.0 %).

Morphology and structure

The topographical characteristics of the organic semiconductor thin films were obtained by Atomic Force Microscopy (AFM) under ambient conditions using a Digital Instruments Dimension 3100 (resonance frequency of 300 kHz, spring constant of 40 N m^{-1}, and tip radius <10 nm). Tapping mode with a scan rate of 1 Hz was used for imaging, and the Nanoscope software was used to analyze the images. The XRD pattern of the thin film was obtained using a Malvern Pan-Alytical Empyrean 3 diffractometer with a CuKα (λ = 1.54178 Å) beam.

Synthesis of iongels and hydrogels

The iongel was prepared from a mixture of PVDF-HFP, which acted as the host matrix, and an ionic liquid ([EMIM][TFSI]) in acetone. PVDF-HFP is a hydrophobic and semi-crystalline copolymer with good film-forming ability.[63] PVDF-HFP was added to acetone at a weight ratio of (1:15) and stirred for 2 h at 50 °C to obtain a homogenous solution. The ionic liquid (ratio of 4:1 w/w with respect to PVDF-HFP) was added to the solution, which was stirred for 2 h at 50 °C. The resulting gel was directly spin-coated (500 rpm, 30s, thickness ~130 µm) onto the device for use as a transistor gating medium. PVA hydrogels were prepared using a freezing/thawing method, which leads to the physical crosslinking of polymer chains without the use of crosslinking agents.[64] 16 wt % PVA was dissolved in deionized (DI) water at 95 °C in an oil bath for 1 h. When the solution became transparent, it was cast into a glass petri dish and kept in a freezer (-15 °C) for 3 h and then at room temperature for 24 h. The resulting gel (thickness ~1000 µm) was cut to desired shapes and swelled in three different solutions:0.5M aqueous NaCl (PVA/W (0.5)), mixture of water/glycerol (50/50) (%v) with a concentration of 0.5 M NaCl (PVA/W+Gl (0.5)), and mixture of water/glycerol solution with concentration of 0.7 M NaCl (PVA/W+Gl (0.7)). The different thicknesses of the gating media are due to the difference in processing: ion-gel electrodes were directly spin-coated on the devices, while hydrogels were applied manually on the devices after casting and solidification on a different substrate. As expected, spin coating led to a significantly lower thickness.

Electrochemical characterization of gels

The electrochemical properties of the iongel and hydrogels were evaluated by Electrochemical Impedance Spectroscopy (from 10^5 Hz to 1 Hz) using a VERSASTAT 4 potentiostat (Princeton Applied Research). To extract the ionic conductivities, an MIM structure was adopted, using gold as the bottom electrode and activated carbon-coated carbon paper as the top electrode (Figure 2a), where gold acted as the working electrode and carbon paper acted as the reference and counter electrodes, respectively. For CV measurements in the transistor configuration, we used a two-electrode configuration, where DPP-DTT films served as the working electrode, carbon paper as the counter and quasi-reference electrodes, and gels as the electrolyte, with a scan rate of 50 mV s^{-1} or 10 mV s^{-1} between -1V and +1 V versus the carbon quasi-reference. The current density in the CV curves was normalized to the geometric area of the semiconductor in contact with the electrolyte.

The ionic conductivities (σ) of the gels were calculated using Equation (1):[41]

$$\sigma = \frac{1}{R_b} . \frac{d}{S} \quad (1)$$

where d (cm) is the thickness of the gel and S (cm^2) is the contact area between the electrode and electrolyte. R_b is the bulk resistance (Ω), which is equal to the value of Z_r in the high-frequency region (10^5 Hz), as shown in Figure 2c. The thicknesses of the gels were measured using optical microscopy.

The specific capacitance (F cm^{-2}) of the gels was obtained using Equation (2):[41]

$$C = \frac{-1}{2\pi f Z_i A} \quad (2)$$

where f (Hz) is the frequency, Z_i (ohm) is the imaginary part of the impedance (from Nyquist plots (Figure 2b)), and A (cm^{-2}) is the area of the activated carbon paper top contact (0.4 cm× 0.8 cm).

Fabrication and characterization of EGTs

Au source and drain electrodes (channel width/length (W/L) = 4000 µm/10 µm) were patterned on Si/SiO_2 and PET substrates by photolithography and lift-off, as reported elsewhere.[6] The DPP-DTT solution (2.5 mg mL^{-1}) in $CHCl_3$ was prepared and stirred overnight at room temperature. DPP-DTT films (thickness 65± 5 nm) were obtained by spin coating the prepatterned substrates (1000 rpm, 1 min), followed by heating at 100 °C for 20 min on a hotplate. The iongel and hydrogels were prepared as previously described and applied to semiconductor-coated electrodes.

Carbon paper coated with activated carbon was used as the gate electrode because of its high surface area, which leads to efficient current modulation.[30] For We used two types of activated carbon inks: a hydrophobic solution of activated carbon (28 mg mL^{-1}) and PVDF (1.4 mg mL^{-1}) in NMP For We ion-gel gated devices, and a hydrophilic solution of activated carbon (28 mg mL^{-1}) and Nafion (2.4 mg mL^{-1}) in isopropyl alcohol. Carbon paper pieces (4×8 mm^2) were coated with activated carbon ink via drop casting and heated at 60 °C for 5 h to remove the solvent. Finally, they were deposited in a gel electrolyte solution.

Transistor characterization was performed using a semiconductor parameter analyzer (Agilent B1500A). The charge carrier mobility (cm^2 V^{-1} s^{-1}) of the devices was obtained from the linear transfer characteristics using Eq. (3):

$$\mu_{lin} = \frac{L\, I_{d,lin}}{W\, e\, p\, V_d} \quad (3)$$

where L is the channel length (10 µm), $I_{d,lin}$ is the drain-source current in the linear region, W is the channel width (4000 µm), e is the elementary charge (1.6×10^{-19} C), V_d is the drain-source voltage, and p is the charge carrier density. p (cm^{-2}) was calculated from the linear transfer characteristics using Equation (4):

$$p = \frac{\int I_{gs} dV_g}{r_v e A} \quad (4)$$

where r_v is the scan rate and A (cm^2) is the electrolyte area in contact with the semiconductor.[65]

We evaluated the hysteresis of the devices using Equation (5):

$$W = |V_{gf}(I_d)| - |V_{gb}(I_d)| \quad (5)$$

where $V_{gf}(I_d)$ and $V_{gb}(I_d)$ are related to the gate voltages in the forward and backward scans at a given drain current.[66]

Author Contributions

Mona Azimi: Formal analysis; investigation; methodology; writing – original draft. Arunprabaharan Subramanian: Formal analysis; validation; review and editing. Francesca Soavi: writing –review and editing. Jiaxin Fan: Formal analysis; investigation during the revision process. Fabio Cicoira: Conceptualization; data curation; funding acquisition; project administration; resources; supervision; validation; writing – review and editing.

Conflicts of interest

The authors declare that they have no conflicts of interest.

Acknowledgements

This work was supported by the Natural Sciences and Engineering Research Council of Canada (NSERC) through a discovery grant, and by Defence Research and Development Canada through an IDEaS Micronet (CFPMN1-008) awarded to the FC. MA and AS are grateful for the financial support from the Institut de l'Energie Trottier for the PhD scholarship. JF acknowledges NSERC for a postdoctoral fellowship. This work was supported by CMC Microsystems through the MNT program.

References

1. N. Wang, A. Yang, Y. Fu, Y. Li and F. Yan, *Acc. Chem. Res.*, 2019, **52**, 277-287.
2. H. Ling, D. A. Koutsouras, S. Kazemzadeh, Y. Van De Burgt, F. Yan and P. Gkoupidenis, *Applied Physics Reviews*, 2020, **7**, 011307.
3. A. Doumbia, J. Tong, R. J. Wilson and M. L. Turner, *Advanced Electronic Materials*, 2021, **7**, 2100071.
4. A. Subramanian, M. Azimi, C. Y. Leong, S. L. Lee, C. Santato and F. Cicoira, *Frontiers in Electronics*, 2022, **3**, 813535.
5. Z. Liu, Z. Yin, J. Wang and Q. Zheng, *Advanced Functional Materials*, 2019, **29**, 1806092.

6. A. Subramanian, M. Azimi, C. Santato and F. Cicoira, *Advanced Materials Technologies*, 2021, 2100843.
7. M. Azimi, A. Subramanian, N. A. Roslan and F. Cicoira, *Journal of Physics: Materials*, 2021, **4**, 024001.
8. W. Huang, J. Chen, G. Wang, Y. Yao, X. Zhuang, R. M. Pankow, Y. Cheng, T. J. Marks and A. Facchetti, *Journal of Materials Chemistry C*, 2021, **9**, 9348-9376.
9. Q. Zhang, F. Leonardi, R. Pfattner and M. Mas-Torrent, *Advanced Materials Interfaces*, 2019, **6**, 1900719.
10. I. Cunha, R. Barras, P. Grey, D. Gaspar, E. Fortunato, R. Martins and L. Pereira, *Advanced Functional Materials*, 2017, **27**, 1606755.
11. J. Jeong, G. C. Marques, X. Feng, D. Boll, S. A. Singaraju, J. Aghassi-Hagmann, H. Hahn and B. Breitung, *Advanced Materials Interfaces*, 2019, **6**, 1901074.
12. F. Zare Bidoky, B. Tang, R. Ma, K. S. Jochem, W. J. Hyun, D. Song, S. J. Koester, T. P. Lodge and C. D. Frisbie, *Advanced Functional Materials*, 2020, **30**, 1902028.
13. C. G. Bischak, L. Q. Flagg and D. S. Ginger, *Advanced Materials*, 2020, **32**, 2002610.
14. Y. J. Jo, J. Ok, S. Y. Kim and T. i. Kim, *Advanced Materials Technologies*, 2021, 2001273.
15. I. Cunha, J. Martins, D. Gaspar, P. G. Bahubalindruni, E. Fortunato, R. Martins and L. Pereira, *Advanced Electronic Materials*, 2021, **7**, 2001166.
16. F. Torricelli, I. Alessandri, E. Macchia, I. Vassalini, M. Maddaloni and L. Torsi, *Advanced Materials Technologies*, 2021, 2100445.
17. J. Ko, X. Wu, A. Surendran, B. T. Muhammad and W. L. Leong, *ACS Applied Materials & Interfaces*, 2020, **12**, 33979-33988.
18. H. Lee, S. Lee, W. Lee, T. Yokota, K. Fukuda and T. Someya, *Advanced Functional Materials*, 2019, **29**, 1906982.
19. Z. Wu, X. Yang and J. Wu, *ACS Applied Materials & Interfaces*, 2021, **13**, 2128-2144.
20. A. Campos, S. Riera-Galindo, J. Puigdollers and M. Mas-Torrent, *ACS applied materials & interfaces*, 2018, **10**, 15952-15961.
21. Q. Zhang, F. Leonardi, S. Casalini, I. Temiño and M. Mas-Torrent, *Scientific reports*, 2016, **6**, 1-10.
22. N. Cherukupally, M. Divya and S. Dasgupta, *Advanced Electronic Materials*, 2020, **6**, 2000788.
23. S. Thiemann, S. Sachnov, S. Porscha, P. Wasserscheid and J. Zaumseil, *The Journal of Physical Chemistry C*, 2012, **116**, 13536-13544.
24. Y. Zhang, Q. Zeng, Y. Shen, L. Yang and F. Yu, *ACS Applied Materials & Interfaces*, 2020, **12**, 56216-56221.
25. Y. Na and F. S. Kim, *Chemistry of Materials*, 2019, **31**, 4759-4768.
26. P. Ghamari, M. R. Niazi and D. F. Perepichka, *Chemistry of Materials*, 2021, **33**, 2937-2947.
27. Y. Lei, B. Wu, W.-K. E. Chan, F. Zhu and B. S. Ong, *Journal of Materials Chemistry C*, 2015, **3**, 12267-12272.
28. Y. Zhang, W. Liu, Y. Liu, C. Wang, G. Zhu and W. Song, *Journal of Materials Chemistry C*, 2021, **9**, 15654-15661.
29. A. Subramanian, M. Azimi, C. Santato and F. Cicoira, *Advanced Materials Technologies*, 2022, **7**, 2100843.
30. J. Sayago, F. Soavi, Y. Sivalingam, F. Cicoira and C. Santato, *Journal of Materials Chemistry C*, 2014, **2**, 5690-5694.
31. A. Allison and H. Andreas, *Journal of Power Sources*, 2019, **426**, 93-96.
32. M. Singh, K. Manoli, A. Tiwari, T. Ligonzo, C. Di Franco, N. Cioffi, G. Palazzo, G. Scamarcio and L. Torsi, *Journal of Materials Chemistry C*, 2017, **5**, 3509-3518.
33. J. Kang, J. Wen, S. H. Jayaram, A. Yu and X. Wang, *Electrochimica Acta*, 2014, **115**, 587-598.
34. X. Wang, C. Gong, D. He, Z. Xue, C. Chen, Y. Liao and X. Xie, *Journal of Membrane Science*, 2014, **454**, 298-304.
35. A. F. Visentin and M. J. Panzer, *ACS applied materials & interfaces*, 2012, **4**, 2836-2839.
36. Y. J. Jo, H. Kim, J. Ok, Y. J. Shin, J. H. Shin, T. H. Kim, Y. Jung and T. i. Kim, *Advanced Functional Materials*, 2020, **30**, 1909707.
37. B. Nketia-Yawson, G. D. Tabi and Y.-Y. Noh, *ACS applied materials & interfaces*, 2019, **11**, 17610-17616.
38. B. Nketia-Yawson, S. J. Kang, G. D. Tabi, A. Perinot, M. Caironi, A. Facchetti and Y. Y. Noh, *Advanced Materials*, 2017, **29**, 1605685.
39. G. Tarabella, C. Santato, S. Y. Yang, S. Iannotta, G. G. Malliaras and F. Cicoira, *Applied Physics Letters*, 2010, **97**, 205.
40. S. H. Kim, K. Hong, W. Xie, K. H. Lee, S. Zhang, T. P. Lodge and C. D. Frisbie, *Advanced Materials*, 2013, **25**, 1822-1846.
41. K. H. Seol, S. J. Lee, K. G. Cho, K. Hong and K. H. Lee, *Journal of Materials Chemistry C*, 2018, **6**, 10987-10993.
42. B. Pal, S. Yang, S. Ramesh, V. Thangadurai and R. Jose, *Nanoscale Advances*, 2019, **1**, 3807-3835.
43. Y. J. Jo, K. Y. Kwon, Z. U. Khan, X. Crispin and T.-i. Kim, *ACS Appl. Mater. Inter.*, 2018, **10**, 39083-39090.
44. J. B. Segur and H. E. Oberstar, *Industrial & Engineering Chemistry*, 1951, **43**, 2117-2120.
45. M. B. A. Rahman, K. Jumbri, M. Basri, E. Abdulmalek, K. Sirat and A. B. Salleh, *Molecules*, 2010, **15**, 2388-2397.
46. M. Di Lauro, M. Berto, M. Giordani, S. Benaglia, G. Schweicher, D. Vuillaume, C. A. Bortolotti, Y. H. Geerts and F. Biscarini, *Advanced Electronic Materials*, 2017, **3**, 1700159.
47. K.-J. Baeg, D. Khim, D.-Y. Kim, J. B. Koo, I.-K. You, W. San Choi and Y.-Y. Noh, *Thin Solid Films*, 2010, **518**, 4024-4029.
48. I. Valitova, P. Kumar, X. Meng, F. Soavi, C. Santato and F. Cicoira, *ACS Applied Materials & Interfaces*, 2016, **8**, 14855-14862.
49. C. Santato, F. Cicoira, P. Cosseddu, A. Bonfiglio, P. Bellutti, M. Muccini, R. Zamboni, F. Rosei, A. Mantoux and P. Doppelt, *Applied physics letters*, 2006, **88**, 163511.
50. R. Morais, D. H. Vieira, M. dos Santos Klem, C. Gaspar, L. Pereira, R. Martins and N. Alves, *Semiconductor Science and Technology*, 2022, **37**, 035007.
51. B. Nketia-Yawson, G. D. Tabi, J. W. Jo and Y. Y. Noh, *Advanced Materials Interfaces*, 2020, **7**, 2000842.
52. N. Delavari, K. Tybrandt, M. Berggren, B. Piro, V. Noël, G. Mattana and I. Zozoulenko, *Journal of Physics D: Applied Physics*, 2021, **54**, 415101.
53. S. J. Lee, K. G. Cho, S.-H. Jung, S. Kim, J.-K. Lee and K. H. Lee, *Macromolecular Research*, 2020, **28**, 683-687.
54. S. H. Kim, K. Hong, K. H. Lee and C. D. Frisbie, *ACS applied materials & interfaces*, 2013, **5**, 6580-6585.
55. V. Kaphle, S. Liu, C. M. Keum and B. Lüssem, *physica status solidi (a)*, 2018, **215**, 1800631.
56. M. J. Panzer and C. D. Frisbie, *J. Am. Chem. Soc.*, 2007, **129**, 6599-6607.

57. C.-h. Kim, M. Azimi, J. Fan, M. Wang, H. Nagarajan and F. Cicoira, *Nanoscale*, 2023.
58. O. Bae and F. S. Kim, *Macromolecular Research*, 2020, **28**, 677-682.
59. K. Hong, D. H. Choo, H. J. Lee, J. Y. Park and J.-L. Lee, *Organic Electronics*, 2020, **87**, 105936.
60. C. C. Shih, W. Y. Lee, C. Lu, H. C. Wu and W. C. Chen, *Advanced Electronic Materials*, 2017, **3**, 1600477.
61. Y. Chen, X. Zhuang, E. A. Goldfine, V. P. Dravid, M. J. Bedzyk, W. Huang, A. Facchetti and T. J. Marks, *Advanced Functional Materials*, 2020, **30**, 2005069.
62. G. Karimi, X. Li and P. Teertstra, *Electrochimica Acta*, 2010, **55**, 1619-1625.
63. Y. Wu, Y. Li, Y. Wang, Q. Liu, Q. Chen and M. Chen, *Journal of Energy Chemistry*, 2021.
64. H. Zhang, H. Xia and Y. Zhao, *ACS Macro Letters*, 2012, **1**, 1233-1236.
65. Y. Xia, J. Cho, B. Paulsen, C. D. Frisbie and M. J. Renn, *Appl. Phys. Lett.*, 2009, **94**, 4.
66. A. Di Bartolomeo, L. Genovese, F. Giubileo, L. Iemmo, G. Luongo, T. Foller and M. Schleberger, *2D Materials*, 2017, **5**, 015014.